β-Sheet core of human prion protein amyloid fibrils as determined by hydrogen/deuterium exchange

Xiaojun Lu*†, Patrick L. Wintrode*, and Witold K. Surewicz*†‡

Departments of *Physiology and Biophysics and †Chemistry, Case Western Reserve University, Cleveland, OH 44106

Edited by Arthur Horwich, Yale University School of Medicine, New Haven, CT, and approved December 4, 2006 (received for review September 25, 2006)

Propagation of transmissible spongiform encephalopathies is associated with the conversion of normal prion protein, PrP^C, into a misfolded, oligomeric form, PrP^{Sc}. Although the high-resolution structure of the PrP^C is well characterized, the structural properties of PrP^{Sc} remain elusive. Here we used MS analysis of H/D backbone amide exchange to examine the structure of amyloid fibrils formed by the recombinant human PrP corresponding to residues 90–231 (PrP90–231), a misfolded form recently reported to be infectious in transgenic mice overexpressing PrP^C. Analysis of H/D exchange data allowed us to map the systematically H-bonded β-sheet core of PrP amyloid to the C-terminal region (staring at residue ≈169) that in the native structure of PrP monomer corresponds to α-helix 2, a major part of α-helix 3, and the loop between these two helices. No extensive hydrogen bonding (as indicated by the lack of significant protection of amide hydrogens) was detected in the N-terminal part of PrP90–231 fibrils, arguing against the involvement of residues within this region in stable β-structure. These data provide long-sought experimentally derived constraints for high-resolution structural models of PrP amyloid fibrils.

prion diseases | transmissible spongiform encephalopathy | amyloid structure | mass spectrometry

Transmissible spongiform encephalopathies (TSEs), also referred to as prion diseases, are a group of fatal neurodegenerative diseases that include kuru and Creutzfeldt–Jakob disease in humans, as well as scrapie, bovine spongiform encephalopathy, and chronic wasting disease in animals (1–6). These highly unusual disorders, which may be sporadic, inherited, or acquired by infection, have attracted enormous attention from both scientists and the general public. Recently, TSEs emerged as a major public health issue because of the epidemic spread of bovine spongiform encephalopathy and indications that this disease may have been transmitted to humans (2, 4).

Regardless of the primary etiology, TSEs are associated with the conversion of the cellular prion protein (PrP), PrP^C, into a misfolded form, PrP^{Sc}. The "protein-only" model proposes that PrP^{Sc} itself is the infectious TSE agent; it is believed to self-perpetuate by a mechanism involving binding to PrP^C and templating autocatalytic conversion of the latter protein to the PrP^{Sc} state (1, 2). Although not universally accepted, the protein-only model of TSEs is supported by a wealth of experimental data (1–7), including recent success in generating infectious PrP^{Sc} *in vitro* (8, 9). Furthermore, the principle that proteins alone can be infectious has been proven in recent studies examining prion-based inheritance in yeast and fungi (10–12).

The mature PrP^C is a 209-residue glycoprotein with a C-terminally attached glycosylphosphatidylinositol anchor. Although PrP^C and PrP^{Sc} appear to have identical covalent structures (13), they differ profoundly in biophysical properties. PrP^C is monomeric, proteinase-sensitive, and soluble in nonionic detergents, whereas PrP^{Sc} is partially resistant to proteinase K (PK) digestion and insoluble, forming aggregates with characteristics often similar to amyloid fibrils (1–6). Recent studies show that the degree of polymerization affects biological properties of the protein, with infectivity residing in oligomeric and not monomeric forms of PrP (14).

These differences in physical properties seem to reflect different conformations of the two PrP isoforms; indeed, low-resolution optical spectroscopic data indicate that PrP^C from normal brain is rich in α-helical structure, whereas PrP^{Sc} contains a high proportion of β-sheet (15, 16). NMR structural studies revealed that the recombinant PrP, a nonglycosylated model of PrP^C, consists of a largely unstructured N-terminal part and a folded C-terminal domain encompassing three α-helices and two very short β-strands, with a disulfide bond bridging helices 2 and 3 (17–19). In contrast to high-resolution data for the monomeric PrP^C, our understanding of the structure of PrP^{Sc} or synthetic PrP^{Sc}-like aggregates is very poor, hindering efforts to understand the molecular basis of the disease. Although new tools have recently emerged for studying the architecture of ordered protein aggregates (20, 21), these newly emerging approaches have not yet been used to probe the structure of mammalian prion amyloids.

Recently it has been shown that the recombinant PrP (PrP23–231), or a biologically relevant fragment, PrP90–231, can be converted into a variety of oligomeric forms that are rich in β-sheet structure and have increased resistance to PK digestion (22–25). These aggregates include amyloid fibrils, a form of PrP recently reported to be infectious in a transgenic mice model overproducing PrP^C (8). Here we have used MS analysis of H/D exchange to probe the structure of amyloid fibrils formed by the recombinant human PrP. This approach allowed us to identify the core of PrP amyloid as defined by systematically H-bonded structure, providing crucial experimentally derived constraints for high-resolution structural models.

Results

Peptide Mapping and Coverage. Tandem MS experiments with native recombinant human PrP fragment 90–231 (huPrP90–231) identified 48 peptic fragments, and a few additional peptides were identified upon reduction of the disulfide bond by using Tris(2-carboxyethyl)phosphine hydrochloride (see *Materials and Methods*). Although some of these peptic fragments could not be separated under the conditions of the rapid HPLC gradient required for hydrogen exchange experiments, we were able to analyze with good signal-to-noise ratio the exchange data for 31 peptides. These fragments cover 96% of the entire huPrP90–231 sequence and, in many regions, have multiple overlaps; the only significant gap encompasses residues 214–217.

Author contributions: X.L., P.L.W., and W.K.S. designed research; X.L. performed research; X.L., P.L.W., and W.K.S. analyzed data; and W.K.S. wrote the paper.

The authors declare no conflict of interest.

This article is a PNAS direct submission.

Abbreviations: TSE, transmissible spongiform encephalopathy; PrP, prion protein; huPrP90–231, recombinant human PrP fragment 90–231; HXMS, H/D exchange combined with MS; PK, proteinase K.

‡To whom correspondence should be addressed at: Department of Physiology and Biophysics, Case Western Reserve University, 2109 Adelbert Road, Cleveland, OH 44106. E-mail: witold.surewicz@case.edu.

© 2007 by The National Academy of Sciences of the USA

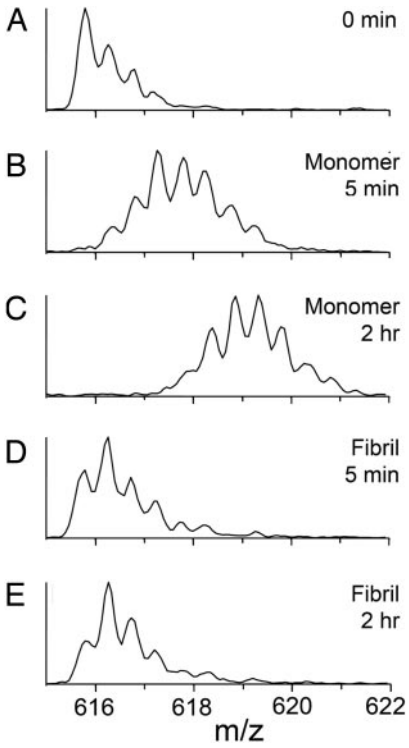

Fig. 1. MS spectra of double-charged peptide 198–207 illustrating time-dependent deuterium uptake. *A* represents nondeuterated reference, and *B–E* represent spectra after 5-min and 2-h exchange in huPrP90–231 monomer and amyloid fibrils.

H/D Exchange Data for the Soluble Monomer. The kinetics of deuterium incorporation was followed for each peptic fragment over the period of 2 h, with the first experimental point measured after 5 min of isotope exchange. Representative MS spectra for doubly charged peptides 198–207 are shown in Fig. 1. The several isotopic lobes (Fig. 1*A*) are due to the Poisson distribution of the natural abundance ^{13}C atoms in the peptide fragment population. Upon deuterium incorporation, the same fragment shifts to higher mass, with the deuterium distribution pattern convoluted with the ^{13}C pattern (Fig. 1 *B–E*). By measuring the centroid mass of the deuterated peptide and subtracting the centroid mass of undeuterated peptide, the total deuterium uptake can be determined.

As shown in Fig. 2, for the protein monomer we observed no measurable protection for the entire region encompassing residues 90–144, with essentially complete exchange for each peptic fragment during the initial 5-min incubation period. In contrast, variable D-labeling kinetic curves were obtained for individual fragments within the C-terminal region beginning at residue 145, with many of these fragments showing a significant degree of protection. Although MS analysis of H/D exchange lacks the spatial resolution of NMR experiments, the present data for huPrP90–231 monomer are fully consistent with the structural data and exchange protection factors reported in previous NMR studies (18, 26). Thus, most peptic fragments for which rapid deuterium incorporation was observed by MS analysis correspond to the largely unstructured N terminus of huPrP90–231 and parts of the C-terminal domain involved in flexible loops, whereas those that show measurable protection encompass H-bonded α-helical regions and/or the second β-strand. No significant protection was detected for the peptic fragment encompassing the first β-strand (residues 128–131) and two peptides (183/184–197) that correspond to the flexible C-terminal part of helix 2. Again, this agrees with the NMR data that show fast H/D exchange in these regions of the PrP at neutral pH (26). This consistency is important because the exchange data for PrP monomer provide a "baseline" for structural interpretation of deuterium incorporation experiments with huPrP90–231 amyloid fibrils.

H/D Exchange on Amyloid Fibrils. As shown previously (25), incubation of huPrP90–231 under the conditions described in *Materials and Methods* resulted in time-dependent conversion of the protein to amyloid fibrils that bind thioflavine T dye. Although variable in length, morphologically these fibrils appeared quite homogenous (Fig. 3*A*). Some of them associated laterally, forming larger polymeric structures.

Investigation by H/D exchange combined with MS (HXMS) revealed a number of major differences in the deuterium incorporation pattern between assembled amyloid structure and monomeric huPrP90–231, providing an important insight into structural organization of PrP amyloid. All peptic fragments derived from the N-terminal part of huPrP90–231 up to residue 168 consistently showed very rapid incorporation of deuterium, reaching >80% labeling (in most cases 85–95%) during the first 5 min of the exchange experiment (Fig. 2). Such fast labeling strongly argues against the presence of any stable H-bonded structures within this part of the PrP chain in amyloid fibrils, although resolution of data for the 90–127 region is limited by the relatively large size of corresponding peptic fragments.

In sharp contrast to the 90–168 region, we observed a very strong protection against D labeling for the C-terminal part of the molecule starting at residue 169 (Fig. 2). All peptic fragments derived from the 169–213 region showed very little (in majority of cases <20%) deuterium incorporation even after 25 h of exchange. This highly protected region most likely represents systematically H-bonded cross-β structure, defining the amyloid core of the PrP (see *Discussion*). Small levels of exchange observed for some peptides in this putative core region could be due to the involvement of some residues in the order–disorder boundaries and/or loop(s) between H-bonded β-strands. Although the N terminus of the exchange-protected region is relatively well defined at residue ≈169, the C terminus is somewhat more ambiguous because of the gap in coverage for amino acid residues 214–217. However, it should be noted that a significant long-term protection was found for the peptic fragment 218–224. Although partial labeling for the latter fragment occurs relatively fast (35% and 47% after 5 min and 1 h, respectively), further deuterium incorporation becomes very slow, remaining at the level <50% even after 25 h of exchange. Such a kinetic pattern could indicate a structural heterogeneity in this region, with a fraction of molecules being readily accessible to D-labeling and another fraction being strongly protected. However, this type of heterogeneity would be reflected in a bimodal distribution of mass peaks, as observed, for example, for some peptic fragments derived from α-synuclein fibrils (27). The lack of bimodal mass distribution in the present study favors an alternative scenario, in which part of the peptic fragment 218–224 belongs to the exchange-protected core and another part undergoes rapid hydrogen exchange. This would map the C terminus of the exchange-protected region to residue ≈221. The color-coded "protection map" that summarizes 25-h exchange data for huPrP90–231 amyloid fibrils is shown in Fig. 4*A*.

Effect of Fibril Annealing on the Pattern of H/D Exchange. Compared with brain PrP^{Sc}, fibrils produced *in vitro* by a spontaneous conversion of the recombinant PrP have a shorter PK-resistant core (28). Recently, Bocharova *et al.* (29) reported that the PK-resistant core of mouse and hamster full-length PrP can be extended to an ≈16-kDa fragment with the N terminus at residue 97. This rearrangement is accomplished by brief exposure of preformed fibrils to elevated temperature (e.g., 80°C) in the

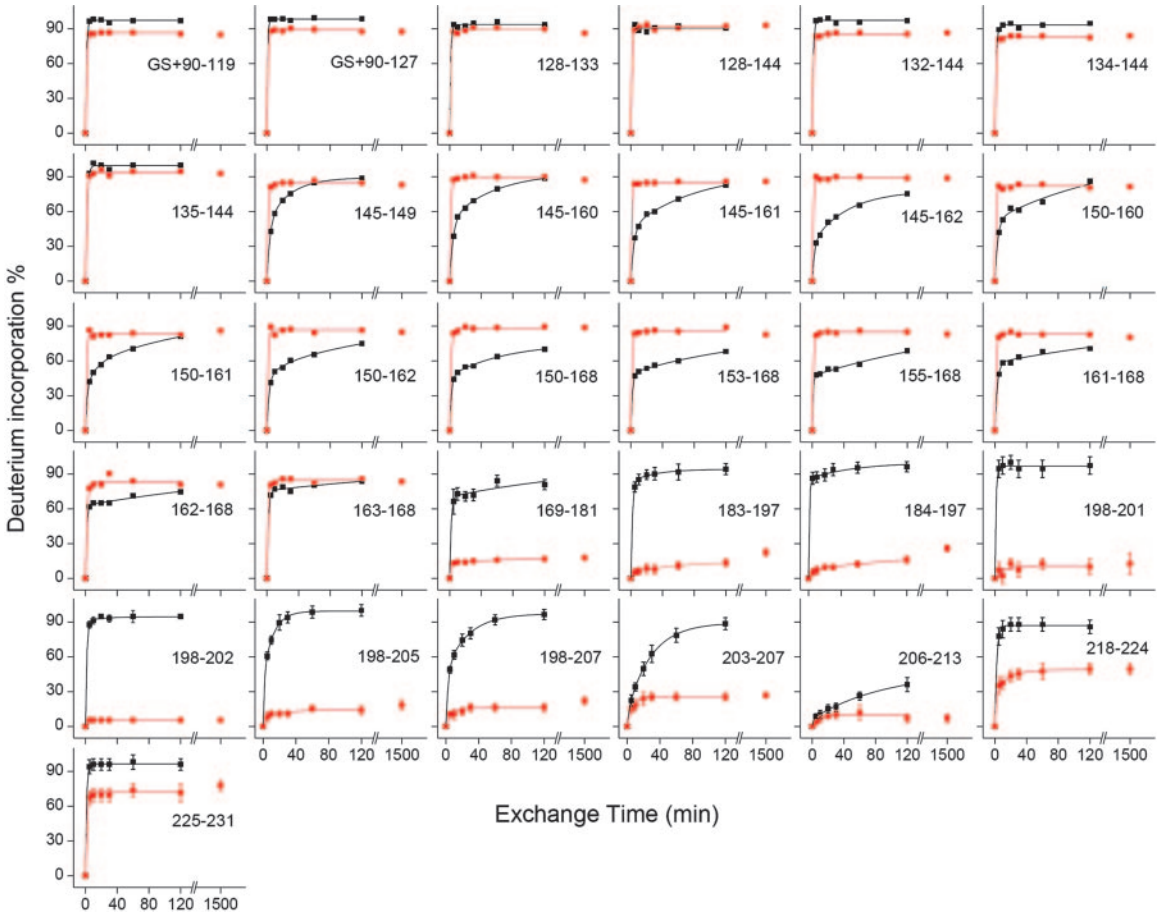

Fig. 2. Kinetic curves for deuterium incorporation by individual peptic fragments for huPrP90–231 monomer (black) and amyloid fibrils (red). The sequence of individual fragments is indicated in each panel. Individual data points and error bars are based on three independent experiments. For clarity of the figure, error bars are shown for selected peptic fragments only; errors for other fragments are of similar magnitude. H/D exchange was performed at 25°C in D_2O buffered with 10 mM phosphate (pD 7.4).

presence of Triton X-100, a procedure referred to as "annealing." We have found that a similar extension of the PK-resistant core occurs upon annealing of fibrils formed by human PrP90–231. As shown in Fig. 3*B*, digestion of nonannealed huPrP90–231 fibrils using low concentrations of PK results in major electrophoretic bands corresponding to ≈10- and 8-kDa fragments. At higher concentrations of the enzyme (above PK:PrP ratio of ≈1:200), the 10-kDa fragment disappears, leaving the sole band at ≈8 kDa. In contrast, the annealed fibrils are significantly more resistant to PK digestion, giving rise to additional electrophoretic bands at ≈15.5 and 16 kDa. Most of these higher-molecular-mass fragments, including a PrP^{Sc}-like band corresponding to 15.5 kDa, persist at least up to a PK:PrP ratio of 1:100.

To gain insight into the structural basis of the annealing process, the annealed fibrils were characterized by HXMS. Surprisingly, the pattern of H/D exchange for PrP90–231 fibrils subjected to annealing was very similar to that described above for nonannealed fibrils (Fig. 4). The only significant difference found was for peptides spanning the short segment between residues 161 and 168, which showed somewhat higher degrees of long-term protection in the annealed fibrils (Fig. 4*B*). However, even in the latter case, the extent of this protection was relatively modest, with ≈60% deuterium incorporation within 25 h. Thus, the region involved in stable systematically H-bonded structure appears to be very similar in the annealed and nonannealed fibrils, indicating that the annealing-induced N-terminal extension of the PK-resistant segment is largely due to conformational rearrangements other than formation of additional β-sheet structure (see *Discussion*).

Discussion

Although major advances have been recently made in TSE research, one of the remaining critical challenges is to determine the high-resolution structure of the infectious PrP^{Sc} conformer. In an effort to bridge this gap, we explored the structural properties of amyloid fibrils formed by the recombinant human PrP corresponding to residues 90–231. This region of PrP is of special importance because it encompasses the entire sequence of PK-resistant brain PrP^{Sc}, contains all known point mutations associated with familial prion diseases, and is sufficient for the propagation of the disease. Recently, Legname *et al.* (8) showed that inoculation of synthetic fibrillar aggregates, similar to those used in the present study, into transgenic mice overexpressing N-terminally truncated PrP^{C} resulted in a TSE disease with very long incubation time, although no infectivity was found in experiments with wild-type mice.

The HXMS method used in this study is a proven tool to explore the structure and dynamics of water-soluble proteins (30). Recently this methodology has been adapted with great success to probe the conformation of fibrillar aggregates that are notoriously difficult to study by most conventional methods (27, 31–33). The H/D exchange approach exploits the fact that backbone amide hydrogens located within the unstructured regions of proteins exchange very rapidly, whereas those in-

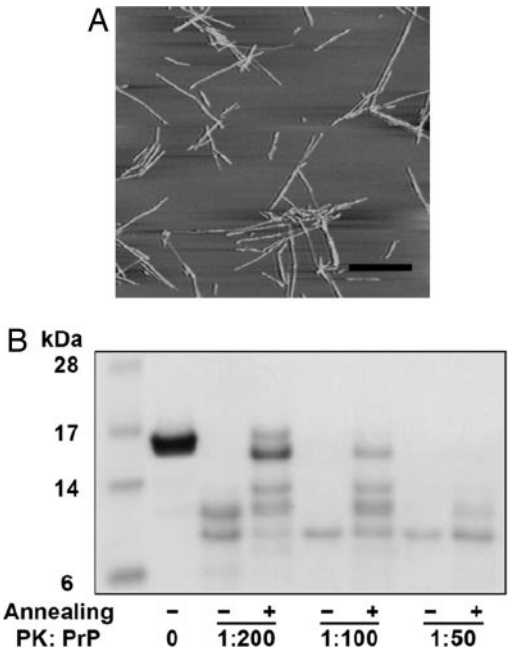

Fig. 3. Characterization of PrP amyloid fibrils. (*A*) Typical amyloid fibrils of huPrP90–231 as seen by atomic force microscopy (amplitude mode). (Scale bar: 1 μm.) (*B*) PK digestion of huPrP90–231 fibrils before and after annealing. Molecular mass markers are shown on the left (first lane), and the ratio of PK:PrP (wt/wt) is indicated below each lane. − and + refer to fibrils before and after annealing, respectively.

volved in systematically H-bonded structures, such as β-sheets and α-helices, usually exchange far more slowly (34). This method is particularly well suited for studying amyloid fibrils because the amide protons in the β-sheet core of fibrillar aggregates are found to be exceptionally resistant to the exchange (27, 31–33, 35, 36).

Our HXMS data reveal that the most highly exchange-protected region in PrP fibrils constitutes a continuous stretch of amides starting at residue 169 and extending to at least residue 213. The C-terminal boundary of this highly protected segment is not as sharply defined as the N terminus because of the gap in coverage between residues 214 and 217. However, data for peptic fragment 218–224 strongly suggest that the amyloid core of PrP90–231, as defined by highly protected H-bonded structure, likely extends as far as to residue ≈221. This region corresponds in the native structure of the PrP monomer to helix 2, a major part of helix 3, and the loop between these two helices (Fig. 4*A*). H/D exchange experiments alone cannot unambiguously discriminate between different types of H-bonded structures. However, the kinetic data in Fig. 2 clearly show that the patterns of D-labeling in the 169–224 region for the monomeric and fibrillar protein are quite different, with long-term protection observed only for amyloid fibrils. Such long-term protection is typical of a cross β-structure, a motif common to many amyloids (27, 31–33, 35, 36). Infrared spectroscopic data indicate that the conversion of PrP23–231 and PrP90–231 to amyloid fibrils is indeed accompanied by a major increase in β-structure (24, 25). This newly formed β-structure is highly unlikely to arise from segments N-terminal to residue ≈169, because all peptic fragments derived from this part of PrP90–231 fibrils show very rapid deuterium incorporation. Thus, the present data strongly indicate that the conversion of PrP to amyloid fibrils involves a major refolding of the C-terminal domain from α-helix to β-structure. The highly exchange-protected β-sheet core of the amyloid reaches from residue 169 to at least 213, likely extending as far as residue 221.

In addition to these changes, there is also a major rearrangement within the region corresponding to the first α-helix in the PrP monomer (residues 145–154). As expected, peptic fragments covering this sequence in PrP^C show a significant degree of protection, especially at shorter exchange times (Fig. 2). This protection disappears in amyloid fibrils, indicating loss of α-helical structure in this part of the protein.

The segment involving residues ≈90–140 is known to be important for the $PrP^C \rightarrow PrP^{Sc}$ conversion (2, 37). The present data do not imply a lack of any structural organization in this part of the PrP90–231 amyloid. However, rapid H/D exchange indicates that any structure existing in this region must be highly dynamic and does not involve extensive, stable backbone H-bonding. In this context one should note that formation of amyloid fibrils has been reported for a number of synthetic peptides derived from PrP90–145 sequence, although often under nonphysiological pH and/or in the presence of organic solvents (38–40). Structurally the best characterized of these is mouse PrP106–126, in which the β-sheet core of the amyloid maps to the central part of the peptide (residues 111–123), including the palindromic sequence VAGAAAAGAV (40). However, our recent experiments show that deletion of this

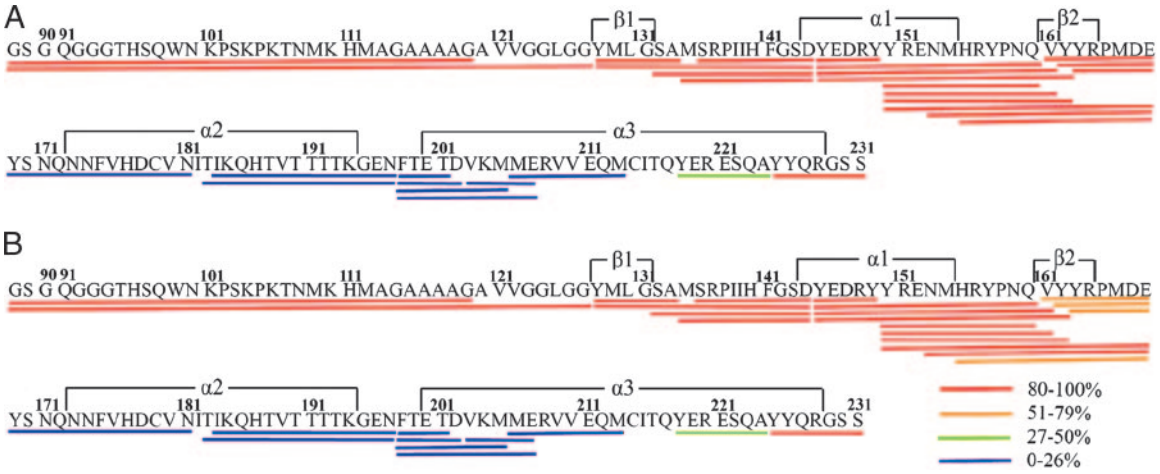

Fig. 4. H/D exchange protection maps summarizing 25-h exchange data for huPrP90–231 fibrils before (*A*) and after (*B*) annealing. Color bars below the sequence represent the percentage of deuterium incorporation. Regions corresponding to α-helices and β-strands in the protein monomer are indicated above the sequence.

sequence has little effect on the ability of both PrP23–231 and PrP90–231 to assemble into amyloid fibrils (K. Surewicz, E. M. Jones, and W.K.S., unpublished data). This, together with the current finding regarding the lack of stable β-sheet structure within the entire 90–145 region of the PrP90–231 amyloid, argues that the structures formed upon conversion of these protein fragments do not necessarily represent those acquired by corresponding sequences during fibrillization of the larger PrP constructs. In a broader context, a wealth of data indicates that self-association into intermolecular β-sheets appears to be a general property of a great many short peptide sequences under the appropriate solvent conditions; we suggest that great caution should be exercised in extrapolating data for these fragments to infer structural properties of fibrils formed by their respective full-length proteins.

The H/D data mapping the N terminus of the β-sheet core in PrP90–231 fibrils to residue ≈169 is generally consistent with the pattern of proteolytic digestion that reveals an ≈8-kDa polypeptide as the most PK-resistant fragment of synthetic PrP fibrils (Fig. 3*B* and ref. 28). The somewhat larger size of this highly PK-resistant fragment as compared with the β-sheet core as identified by H/D exchange data is likely due to protease specificity as well as potential steric constrains. Bocharova *et al.* (28) mapped the N terminus of this 8-kDa fragment to residue 162, and that of a somewhat less PK-resistant 10-kDa fragment to residue 152/153. Although the latter fragments are remarkably similar to a minor population of PK-resistant fragments identified recently in brains of subjects with sporadic Creutzfeldt–Jakob disease (41), they are much shorter than a typical PK-resistant core of PrP^{Sc} (2–4). A recent significant development was the finding that, upon incubation at elevated temperatures in the presence of Triton X-100, the PK-resistant core of recombinant PrP amyloid fibrils may be extended to an ≈16-kDa fragment starting at residue ≈97 (29). We were able to reproduce this observation using huPrP90–231 fibrils. However, to our surprise, we found that annealing has very little effect on the pattern of deuterium incorporation, with HXMS data indicating very similar systematically H-bonded cores in both fibril types. Although proteinase-resistant regions in fibrillar aggregates are typically assumed to reflect cross-β-structure, the present data indicate that this scenario is not necessarily universally valid. Clearly, partial protection from digestion may be also acquired by regions lacking extensive backbone H-bonds and, thus, ordered secondary structure. We suggest that, in the case of annealed PrP fibrils, this is due to changes in the tertiary and/or quaternary structure resulting in steric constraints that prevent access of a large enzyme such as PK (molecular mass ≈ 29 kDa) to potential cleavage sites.

Fibrils used in this study were obtained from a highly purified recombinant PrP, whereas the $PrP^{C}\rightarrow PrP^{Sc}$ conversion *in vivo* occurs in the presence of many cellular cofactors. Some of these cofactors could modulate the final conformation of PrP^{Sc}, especially in the apparently less ordered N-terminal part of the PK-resistant region. Conformational plasticity in this part of PrP^{Sc} appears to underlie the phenomenon of TSE strains, with individual strains corresponding to distinct PrP^{Sc} cleavage sites (2–4). Therefore, although the present data argue against the presence of stable β-sheet structure in the N-terminal part of PrP90–231 amyloid, it is not inconceivable that segment(s) within this region could fold into such a structure in some strains of brain PrP^{Sc}.

Guided by electron microscopic images of 2D crystals, Govaerts *et al.* (42) recently proposed a structural model for PrP^{Sc} in which residues 89–175 form left-handed β-helices that associate into trimers, whereas the entire C-terminal region retains the native α-helical conformation of PrP^{C}. Another model, based on molecular dynamics simulations, postulates that the β-structure core of PrP protofibrils is composed of a three-stranded sheet, E1–E3 (residues 116–119, 119–132, and 160–164), and an isolated strand, E4 (residues 135–140), with three native α-helices being largely preserved (43). The present experimental data (mapping the β-sheet core of PrP90–231 amyloid to the C-terminal region and showing that no systematically H-bonded structure exists within the 90–168 segment) is clearly at odds with both of these *in silico* models. On the other hand, our findings are generally consistent with molecular dynamics simulations by Dima and Thirumalai (44). The latter study predicted the two C-terminal α-helices as the most likely region to undergo a transition to β-structure, although it stopped short of proposing any specific structural model. Further studies are required to elucidate tertiary and quaternary interactions in the recombinant PrP fibrils, as well as to establish a relationship between the structure of these fibrils and that of brain PrP^{Sc}. The present data regarding the systematically H-bonded β-sheet core in PrP amyloid bridge a major gap, providing long-sought experimentally derived constraints for high-resolution structural models.

Materials and Methods

Protein Purification. The plasmid encoding huPrP90–231 with an N-terminal linker containing a His-6 tail and a thrombin cleavage site was described previously (45). The protein was expressed, cleaved with thrombin, and purified according to the previously described protocol (45); it was stored frozen in 10 mM sodium acetate buffer (pH 4).

Preparation and Characterization of Amyloid Fibrils. huPrP90–231 amyloid fibrils were prepared essentially as described previously (25). Briefly, the monomeric protein from a stock solution was diluted to a concentration of 0.7 mg/ml in 50 mM phosphate buffer containing 2 M GdnHCl and adjusted to a final pH of 7.5. The samples were placed in 1.5-ml conical tubes filled to the volume of ≈1 ml and incubated at 37°C with continuous rotation at 8 rpm (Model 400110 Thermolyne Labquake rotator; Barnstead International, Dubuque, IA). The formation of amyloid fibrils was followed by a fluorimetric thioflavine T assay as described previously (25). Once the reaction was completed, samples were analyzed by atomic force microscopy (46).

Freshly prepared huPrP90–231 fibrils were subjected to the so-called annealing process that converts fibrils to a more PK-resistant structure as described previously (29). To this end, preformed fibrils were dialyzed from the denaturant against 10 mM phosphate buffer (pH 7.5) followed by incubation for 15 min at 80°C in the presence of 1% Triton X-100. The sensitivity of annealed and nonannealed fibrils to PK digestion was probed by incubating fibrillar protein (0.3 mg/ml) for 1 h at 37°C with different concentrations of PK in 50 mM phosphate buffer (pH 6.5). The digestion was stopped by addition of PMSF immediately followed by boiling for 15 min in sample buffer containing 2.25 M urea. Samples were analyzed by SDS/PAGE using 12% NuPage gels (Invitrogen, San Diego, CA) and Coomassie blue staining.

H/D Exchange. Fibrils were collected by centrifugation in an Eppendorf tube (6,000 × *g* for 10 min) and washed four to five times with 10 mM phosphate buffer (pH 7.4) to remove GdnHCl, residual nonfibrillar material, and, in the case of fibrils subjected to annealing, most of the detergent. To initiate deuterium labeling, the final pellet (50 μl) was resuspended in 1 ml of D_2O buffer (10 mM phosphate, pD 7.4) and incubated at 25°C from 5 min to 25 h. At various time points fibrils were collected by centrifugation at 16,000 × *g* for 30 sec (to a final volume of ≈50 μl) and rapidly dissociated by adding 500 μl of an ice-cold solution of 7.2 M GdnHCl in an exchange quench buffer (0.1 M phosphate, pH 2.5). The samples (≈0.5 mg of protein per milliliter) were then immediately diluted 10 times with an ice-cold 0.05% TFA in H_2O and digested for 5 min with pepsin

(a huPrP90–231:pepsin ratio of 1:1, wt/wt). The peptic fragments were collected in a peptide microtrap, washed for 5 min to remove salts, and eluted on a C18 HPLC column using a gradient of 2–30% acetonitrile at a flow rate of 50 μl/min (total elution time of 13 min). Peptides separated on the column were analyzed by a Finnigan LCQ-DECA quadruple ion-trap mass spectrometer (ThermoElectron, San Jose, CA) directly coupled to the HPLC system. To slow back-exchange during this procedure, the trap and C18 column were immersed in ice.

Peptide masses were calculated from the centroid of the isotopic envelope by using MagTran software, and the extent of deuterium incorporation at each time point was determined from the shift in mass of labeled peptides relative to unlabeled peptides. To correct for the 5% H_2O present during the exchange-in and for deuterium back-exchange during proteolysis, HPLC separation, and MS analysis, control experiments were performed by using fully deuterated protein prepared by 2-h incubation in 6 M guanidine deuterochloride in D_2O/H_2O (95:5, vol/vol) buffered with 10 mM potassium phosphate (pD 7.2). The average level of deuterium retention in the fully deuterated reference sample was ≈60%. The extent of deuterium incorporation in a given peptide (corrected for back exchange) was calculated as $D/N = [m(t) - m(0\%)]/[m(100\%) - m(0\%)]$, where $m(t)$ is the observed centroid mass of the peptide at time point t, $m(0\%)$ is the measured mass of an undeuterated reference sample, $m(100\%)$ is the observed mass of a fully deuterated reference sample, N is the total number of exchangeable amide protons in a given peptide, and D is the number of amide hydrogen atoms incorporated in each peptic fragment.

Exchange experiments with monomeric huPrP90–231 were performed similarly, starting with a small volume of 10 mg/ml solution of the protein in 10 mM acetate buffer (pH 4) and diluting it 20 times in D_2O buffered with 10 mM phosphate (pD 7.4). To mimic the digestion conditions of amyloid fibrils, the exchange reaction was quenched by using ice-cold 0.1 M phosphate buffer (pH 2.3) containing 0.65 M GdnHCl.

PrP contains two disulfide-linked Cys residues at positions 179 and 214. To improve sequence coverage in the region containing these residues, an additional series of experiments was performed in which, after H/D exchange, the native disulfide bond was rapidly reduced by treatment with 0.1 M Tris(2-carboxyethyl)phosphine hydrochloride in the quench buffer containing 7.2 M GdnHCl. Peptic digestion was then performed on the reduced protein. This procedure allowed us to extend deuterium exchange studies to a peptide fragment encompassing residues 169–181.

Peptide Mapping. Before H/D exchange experiments, pepsin digestion fragments were identified by a standard procedure involving separation on a C18 HPLC column coupled to a Finnigan LCQ quadrupole ion-trap mass spectrometer, sequencing by tandem MS, and analysis using the SEQUEST search algorithm (ThermoElectron) and manual inspection. Additionally, peptide identification was confirmed by exact mass measurements by using Fourier Transform Ion Cyclotron Resonance MS (LTQ-ICR; ThermoElectron).

This work was supported by National Institutes of Health Grant NS 44158.

1. Prusiner SB (1982) *Science* 216:136–144.
2. Prusiner SB (1998) *Proc Natl Acad Sci USA* 95:13363–13383.
3. Caughey B, Chesebro B (2001) *Adv Virus Res* 56:277–311.
4. Collinge J (2001) *Annu Rev Neurosci* 24:519–550.
5. Aguzzi A, Polymenidou M (2004) *Cell* 116:313–327.
6. Weissmann C (2004) *Nat Rev Microbiol* 2:861–871.
7. Surewicz WK, Jones EM, Apetri AC (2006) *Acc Chem Res* 39:654–662.
8. Legname G, Baskakov IV, Nguyen HO, Riesner D, Cohen FE, DeArmond SJ, Prusiner SB (2004) *Science* 305:673–676.
9. Castilla J, Saa P, Hetz C, Soto C (2005) *Cell* 121:195–206.
10. Chien P, Weissman JS, DePace AH (2004) *Annu Rev Biochem* 73:617–656.
11. Uptain SM, Lindquist S (2002) *Annu Rev Microbiol* 56:703–741.
12. Brachmann A, Baxa U, Wickner RB (2005) *EMBO J* 24:3082–3092.
13. Stahl N, Baldwin MA, Teplow DB, Hood L, Gibson BW, Burlingame AL, Prusiner SB (1993) *Biochemistry* 32:1991–2002.
14. Silveira JR, Raymond GJ, Hughson AG, Race RE, Sim VL, Hayes SF, Caughey B (2005) *Nature* 437:257–261.
15. Caughey BW, Dong A, Bhat KS, Ernst D, Hayes SF, Caughey WS (1991) *Biochemistry* 30:7672–7680.
16. Pan KM, Baldwin M, Nguyen J, Gasset M, Serban A, Groth D, Mehlhorn I, Huang Z, Fletterick RJ, Cohen FE, *et al*. (1993) *Proc Natl Acad Sci USA* 90:10962–10966.
17. Riek R, Hornemann S, Wider G, Billeter M, Glockshuber R, Wuthrich K (1996) *Nature* 382:180–182.
18. Zahn R, Liu A, Luhrs T, Riek R, von Schroetter C, Lopez Garcia F, Billeter M, Calzolai L, Wider G, Wuthrich K (2000) *Proc Natl Acad Sci USA* 97:145–150.
19. Donne DG, Viles JH, Groth D, Mehlhorn I, James TL, Cohen FE, Prusiner SB, Wright PE, Dyson HJ (1997) *Proc Natl Acad Sci USA* 94:13452–13457.
20. Tycko R (2004) *Curr Opin Struct Biol* 14:96–103.
21. Nelson R, Eisenberg D (2006) *Curr Opin Struct Biol* 16:260–265.
22. Swietnicki W, Morillas M, Chen SG, Gambetti P, Surewicz WK (2000) *Biochemistry* 39:424–431.
23. Baskakov IV, Legname G, Baldwin MA, Prusiner SB, Cohen FE (2002) *J Biol Chem* 277:21140–21148.
24. Bocharova OV, Breydo L, Parfenov AS, Salnikov VV, Baskakov IV (2005) *J Mol Biol* 346:645–659.
25. Apetri AC, Vanik DL, Surewicz WK (2005) *Biochemistry* 44:15880–15888.
26. Calzolai L, Zahn R (2003) *J Biol Chem* 278:35592–35596.
27. Del Mar C, Greenbaum EA, Mayne L, Englander SW, Woods VL, Jr (2005) *Proc Natl Acad Sci USA* 102:15477–15482.
28. Bocharova OV, Breydo L, Salnikov VV, Gill AC, Baskakov IV (2005) *Protein Sci* 14:1222–1232.
29. Bocharova OV, Makarava N, Breydo L, Anderson M, Salnikov VV, Baskakov IV (2006) *J Biol Chem* 281:2373–2379.
30. Wales TE, Engen JR (2006) *Mass Spectrom Rev* 25:158–170.
31. Kheterpal I, Zhou S, Cook KD, Wetzel R (2000) *Proc Natl Acad Sci USA* 97:13597–13601.
32. Nazabal A, Maddelein ML, Bonneu M, Saupe SJ, Schmitter JM (2005) *J Biol Chem* 280:13220–13228.
33. Kheterpal I, Wetzel R (2006) *Acc Chem Res* 39:584–593.
34. Krishna MM, Hoang L, Lin Y, Englander SW (2004) *Methods* 34:51–64.
35. Hoshino M, Katou H, Hagihara Y, Hasegawa K, Naiki H, Goto Y (2002) *Nat Struct Biol* 9:332–336.
36. Ritter C, Maddelein ML, Siemer AB, Luhrs T, Ernst M, Meier BH, Saupe SJ, Riek R (2005) *Nature* 435:844–848.
37. Muramoto T, Scott M, Cohen FE, Prusiner SB (1996) *Proc Natl Acad Sci USA* 93:15457–15462.
38. Tagliavini F, Prelli F, Verga L, Giaccone G, Sarma R, Gorevic P, Ghetti B, Passerini F, Ghibaudi E, Forloni G, *et al*. (1993) *Proc Natl Acad Sci USA* 90:9678–9682.
39. Nguyen JT, Inouye H, Baldwin MA, Fletterick RJ, Cohen FE, Prusiner SB, Kirschner DA (1995) *J Mol Biol* 252:412–422.
40. Kuwata K, Matumoto T, Cheng H, Nagayama K, James TL, Roder H (2003) *Proc Natl Acad Sci USA* 100:14790–14795.
41. Zou WQ, Capellari S, Parchi P, Sy MS, Gambetti P, Chen SG (2003) *J Biol Chem* 278:40429–40436.
42. Govaerts C, Wille H, Prusiner SB, Cohen FE (2004) *Proc Natl Acad Sci USA* 101:8342–8347.
43. DeMarco ML, Daggett V (2004) *Proc Natl Acad Sci USA* 101:2293–2298.
44. Dima RI, Thirumalai D (2004) *Proc Natl Acad Sci USA* 101:15335–15340.
45. Morillas M, Swietnicki W, Gambetti P, Surewicz WK (1999) *J Biol Chem* 274:36859–36865.
46. Jones EM, Surewicz WK (2005) *Cell* 121:63–72.